A domain decomposition method for solution of a PDE-constrained generalized Nash equilibrium model of biofilm community metabolism

Isaac Klapper, Daniel B. Szyld, Yinli Yu,
Karsten Zengler, Tianyu Zhang, and Cristal Zúñiga

Report 22-07-25
July 2022. Revised June 2023 and October 2023

Department of Mathematics
Temple University
Philadelphia, PA 19122

This report is available in the World Wide Web at
`http://www.math.temple.edu/~szyld`

A DOMAIN DECOMPOSITION METHOD FOR SOLUTION OF A PDE-CONSTRAINED GENERALIZED NASH EQUILIBRIUM MODEL OF BIOFILM COMMUNITY METABOLISM*

ISAAC KLAPPER†, DANIEL B. SZYLD†, XINLI YU†, KARSTEN ZENGLER‡, TIANYU ZHANG§, AND CRISTAL ZÚÑIGA¶

Abstract. Microbes are able to deploy different strategies in response to, and depending on, local environmental conditions. In the setting of a microbial community, this property induces a Nash equilibrium problem because access to environmental resources is bounded. If microbes are also distributed in space, then those resources are subject to transport limitations (encoded in a PDE) and so microbial strategies at one location influence resources, and hence microbial strategies, at another. Here we formulate the resulting PDE-coupled generalized Nash equilibrium problem for a multispecies biofilm community, and propose a domain decomposition-based method for its solution. An example consisting of a model with two microbial species biofilm with 33 externally transported chemical concentrations is presented.

Key words. Biofilms, microbial metabolism, generalized Nash equilibrium, domain decomposition

MSC codes: 92D25, 91A13, 65N55

1. Introduction.

There exist many systems in which multiple "players", each with their own set of possible strategies and objectives, interact with one another in some manner. Individual players hope to choose a strategy from their allowable strategy sets which will be most beneficial for themselves; however their outcomes depend on choices of others. In the case that each player has chosen a strategy such that no one of them can improve their individual outcome by a change to (only) their own strategy, a *Nash equilibrium* has occurred. If it happens that players' strategy sets depend on other players' strategy choices, a *generalized Nash equilibrium* problem results [11]: is it possible for every player, simultaneously, to choose their own allowable strategy such that no one of them would be advantaged by changing to a different allowable strategy (under the condition that all others' choices are unchanged), despite having an allowable strategy set which depends on other players' choices?

In this context, we consider communities of microrganisms (the players), in which individual microorganism tune their own metabolisms (the strategies) in response to the local environment, specifically extracellular concentrations of substrates and other chemicals, and in turn and in consequence changing those concentrations [35]. (*Metabolism*: the chemical reactions within cells that extract energy and produce cell material.) We can hypothesize that the resulting metabolic choices will approach a Nash equilibrium state. Determination of those metabolic strategies is, generally, a generalized Nash equilibrium problem (GNEP), as each organism determines its metabolic strategy in response to environmental conditions while simultaneously influencing those conditions. Allowable metabolic choices, which depend on environmental conditions at steady state, are thus not evident in advance.

Metabolic choices are subject to chemical fluxes into and out of cells [37], which in

*This version dated October 18, 2023

†Department of Mathematics, Temple University (038-16), Philadelphia, PA

‡Departments of Pediatrics and Bioengineering, University of California, San Diego, CA

§Department of Mathematical Sciences, Montana State University, Bozeman, MT

¶Department of Biology, San Diego State University, San Diego, CA

turn are constrained by chemical fluxes into and out of, and through, the extracellular environment. Such constraints can be more complex when, as is often the case, the community is not well mixed so that the metabolism is coupled to spatial dependence of external chemical concentrations, i.e., metabolism is coupled to an accompanying transport equation [47]. The result is a PDE-constrained GNEP in which player strategies translate into source and sink terms in an equation balancing chemical concentration fluxes over a spatial domain.

A common example of spatially structured microbial communities are biofilms, collections of sessile microorganisms bound together by a self-secreted matrix of extracellular polymers that are well known to exhibit complex, spatially distributed metabolic activity [40]. Indeed, it is likely that biofilm spatial structure is a consequence of diffusive transport limitation – activity is necessarily constrained by the rates at which substrates can be gathered and byproducts can be removed. If, as is often the case, a given biofilm system can be approximated to be in a metabolic steady state, the result is effectively a GNEP coupled to a set of reaction-diffusion equations (for chemical concentrations). The aim here is to formulate such a system together with a numerical method for its solution.

To compute these coupled equilibria, we employ an iterative method in which microbial players update their metabolic strategies at each iteration. However, it turns out that the coupling with reaction-diffusion equations can be rather stiff: changes of metabolic strategy at one location in the biofilm can cause significant changes in chemical concentrations at distant locations, leading to numerical instability. In response, we introduce an overlapping domain decomposition method (cf. [39, 42]) which, by dint of iterating on small subdomains, alleviates stiffness issues. We mention that domain decomposition ideas have been applied to PDE-constraint optimization; see, e.g., [6, 31, 32, 44], where Schwarz methods are used as preconditioners. Here we use them directly as a solver. To our knowledge, this is the first time that domain decomposition methods have been used to solve this type of differential equations directly and in particular to handle stiff problems.

Results presented build on previous work [47]; here the connection between microbial community metabolism and GNEPs is made and demonstrated using full scale microbial metabolisms. To do so, we introduce a domain decomposition approach capable of solving the resulting problems even for fully developed biofilms. We note further that a domain decomposition platform is naturally parallelizable, potentially an advantage when pointwise optimization computations are expensive as they can be for metabolic calculations. Asynchronous parallel methods [14, 13, 24] are also possible.

In this study, we couple flux balance analysis (FBA), a technique for modeling microbial metabolism [29], with a continuum model at the community (or environmental) scale. FBA is used here to generate metabolic strategy choices from the set of allowable strategies; other methods could be employed instead, as in [47] for example. There is some history of coupling FBA and related metabolic modeling methods with environmental models, sometimes termed dynamic flux balance analysis [25], see for example [7, 15, 18, 30, 41], though the connection to GNEPs has not been considered. Conversely, linking microbial interactions to game theory ideas, including in spatially structured communities, is not in itself a new idea (see, e.g., [12, 16, 23, 43]); here we make the connection of metabolism to a PDE-constrained GNEP together with a suggested method for computing solutions.

The rest of the paper is organized as follows. In Section 2, a microbial commu-

nity GNEP is presented in a relatively general equation form, and the connection to metabolism, and metabolic choices, is specified. The next task is development of a numerical method for its solution. At this point we restrict to a 1D domain. Computationally, this is a significant simplification, but note that 1D domains are still important biologically, particularly for biofilms, for which much of the most important structure and function arises from variation in the "depth" direction as a consequence of diffusive transport limitation. In Section 3, then, we introduce a proposed numerical method, based on a combination of a Green's function solver with domain decomposition, for the solution of the microbial community GNEP. This choice is motivated by efficiency but also by stiffness issues which arises in diffusion-limited systems where sharp exponential drop-offs (in space) can occur. Such drop-offs are notably common in biofilms, indeed they are the norm, and result often in microenvironments called active layers that can dominate biofilm ecology and function [40].

The final two sections are devoted to numerical computations. In Section 4 we use a simple example to illustrate how, beyond the known potential for efficiency, domain decomposition also helps with handling stiff differential equations of the sort that arise in biofilm models. This same example can also be viewed as a toy model for a biofilm computation as it illustrates formation of a sharp active layer. Then, in Section 5, the developed methodology is applied in a biofilm context. We couple a standard community-scale biofilm model to FBA driven genome-scale metabolic models. The result is a much more realistic model of biofilm ecology. At the same time, though, it is also much more computationally challenging. FBA computations involve, by themselves, moderately large optimization calculations, and the coupling to a biofilm model in turn requires large numbers of such optimizations. We demonstrate that the presented methodology is able to handle the overall computation. In summary, we are able to pose microbial community ecology models, biofilms specifically, as PDE-constrained GNEPs, and to solve a non-trivial example using a novel application of domain decomposition methods for computing the solution of the stiff problems.

2. Problem formulation. We consider GNEPs associated with microbial community models. At their core are transport equations of the form

$$\mathcal{L}_j\, C_j(\mathbf{x}) = -f_j(C_1(\mathbf{x}), C_2(\mathbf{x}), \ldots, C_n(\mathbf{x}); V_1(\mathbf{x}), V_2(\mathbf{x}), \ldots, V_m(\mathbf{x})) \qquad (2.1)$$

for $\mathbf{x}$ in a domain $\Omega \subset \mathbb{R}^3$, and where $C_j(\mathbf{x})$, $j = 1, 2, \ldots n$, are chemical concentrations. The transport operators $\mathcal{L}_j$ are here supposed to be $\nabla \cdot (\kappa \nabla \cdot)$ (though we will later set κ to be constant), i.e., a diffusion operator, but in some instances can be more general including for example advective transport. The functions $V_\ell(\mathbf{x})$, $\ell = 1, 2, \ldots, m$, are volume fractions of the species present, which can be microbial or other quantities, e.g., water. Boundary conditions typically consist of a mix of homogeneous Neumann (i.e., no-flux) together with homogeneous or non-homogeneous Dirichlet conditions.

Equations (2.1) have a solution when operators $\mathcal{L}_j$ is invertible under reasonable conditions on the functions f_j (e.g., bounded and smooth, see for example [10]). Hence we see that the associated GNEP has a solution. Solution uniqueness however is less clear, and is not addressed here. Note also that in practice, in the metabolic application we consider, in fact functions f_j may only be piecewise smooth, reflecting the possibility that metabolic choices can change abruptly with small changes in extracellular chemical concentrations (for example, a switch between aerobic and anaerobic metabolism at a critical oxygen concentration). In the community context, discontinuities may be mollified by metabolic variation within neighboring cells, effectively

smoothing metabolic switching. That is, variations among cells, even of the same species, may result in locally smoothed resource uptake. For example, even cell size differences might influence maximum uptake rate. In any case, we discuss existence of solutions in the Appendix.

Functions f_j, $j = 1, 2, \ldots n$, indicate flux of chemicals into or out of microbes, and are assumed of the form

$$f_j(\mathbf{C}; \mathbf{V}) = \sum_{\ell=1}^{m} F_{j\ell}(\mathbf{C}) V_\ell, \tag{2.2}$$

with $\mathbf{C}$ and $\mathbf{V}$ being vectors whose components are C_j, $j = 1, 2, \ldots n$, and V_ℓ, $\ell = 1, 2, \ldots m$, respectively. Function $F_{j\ell}$ is flux of chemical j out of species ℓ. We assume that each $F_{j\ell}$ is well-defined, that is, given chemical concentration profile $\mathbf{C}(\mathbf{x})$, flux $F_{j\ell}(\mathbf{x})$ is uniquely determined. Vector

$$S_\ell(\mathbf{x}) = [\, F_{1\ell}(\mathbf{C}(\mathbf{x}))\ F_{2\ell}(\mathbf{C}(\mathbf{x}))\ \ldots\ F_{n\ell}(\mathbf{C}(\mathbf{x}))]$$

is then, in the language of GNEPs, the strategy chosen by species ℓ at location $\mathbf{x}$. The strategy set for species ℓ at location $\mathbf{x}$ consists of allowable choices for $\mathcal{S}_\ell(\mathbf{x})$, and is, generally, constrained by $\mathbf{C}(\mathbf{x})$ and hence coupled to those strategy choices made by other species and in other locations through equations (2.1). An example of the constraints imposed on S_ℓ by concentrations $\mathbf{C}$ is provided below.

3. Numerical Methods. For simplicity we restrict to a one dimensional domain $\Omega = [0, L]$ with spatially independent diffusivity, for which equations (2.1) reduce to

$$\kappa_j \frac{d^2}{dz^2} C_j(z) = -f_j(\mathbf{C}(z); \mathbf{V}(z)). \tag{3.1}$$

Boundary conditions for (3.1) are combinations of Dirichlet (homogeneous or nonhomogeneous) and Neumann (homogeneous only, typically but not necessarily). The methodology described below naturally extends to higher dimensions.

The domain $[0, L]$ is discretized using p overlapping intervals with minimum overlap, that is, with only one mesh point from the neighboring interval, as shown in Figure 3.1. To be more precise, $[0, L]$ is discretized into p subintervals, each with N interior meshpoints plus one additional mesh point on the left and the right, with intervals sharing two meshpoints with each neighbor. We employ a typical domain decomposition approach, also called a Schwarz method, often used as a preconditioner for discretizations of partial differential equations; see, e.g., [39, 42].

For each subinterval $[z_{l_i}, z_{r_i}]$, $i = 1, \ldots, p$ (with $z_{l_1} = 0$, and $z_{r_p} = L$), let $C_j^{(i)}$ satisfy the second order boundary value problem

$$\kappa_j \frac{d^2}{dz^2} C_j^{(i)}(z) = -f_j(\mathbf{C}^{(\mathbf{i})}(z); \mathbf{V}(z)), \tag{3.2}$$

with boundary conditions $C_j^{(i)}(z_{l_i}) = C_j^{(i-1)}(z_{l_i})$, $i = 2, \ldots, p$, $C_j^{(i)}(z_{r_i}) = C_j^{(i+1)}(z_{r_i})$, $i = 1, \ldots, p-1$. In words, for interior interval overlaps, concentrations have to match at each of the two overlapping discretization points. At the two domain end points, in the case of Dirichlet boundary conditions, $\mathbf{C}^{(1)}(0) = \mathbf{A}$ and, $\mathbf{C}^{(p)}(L) = \mathbf{B}$ (different boundary conditions are treated similarly, though Neumann boundary conditions on both ends requires a somewhat modified method). Thus, we have p coupled second order boundary value problems in smaller intervals. Following Schwarz iteration,

solutions to (3.2) for all subintervals and all chemical concentrations are approximated, updated boundary values are exchanged, and the process is repeated until a stopping condition is met. The Schwarz decomposition serves two main purposes. First, as will be seen below, it promotes numerical stability. Second, it provides a natural platform for parallelization, though we do not explore this feature here.

We mention that a proof of convergence for this overlapping domain decomposition method with Dirichlet boundary conditions goes back to Schwarz in 1870 for partial differential equations; see, e.g., [42]. That proof carries over directly to our situation in the continuous case. We discuss the appropriate discretized version below.

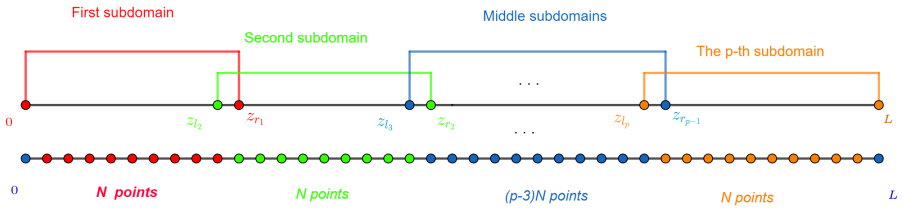

FIG. 3.1. *Representation of the discretization with p overlapping intervals*

Numerically, approximation of the solution of equations (3.1) proceeds as follows. First, the system is recast into homogeneous boundary condition form by introducing new unknown subinterval functions $\mathbf{D}^{(i)}$ according to

$$\mathbf{D}^{(i)}(z) = \mathbf{C}^{(i)}(z) - \mathbf{h}^{(i)}(z), \tag{3.3}$$

with

$$\mathbf{h}^{(i)}(z) = \frac{1}{z_{\ell_i} - z_{r_i}}(z_{\ell_i}\mathbf{B^{(i)}} - z_{r_i}\mathbf{A^{(i)}} + (\mathbf{A^{(i)}} - \mathbf{B^{(i)}})z) \tag{3.4}$$

where $\mathbf{A^{(i)}}, \mathbf{B^{(i)}}$ are boundary conditions for $\mathbf{C}^{(i)}(z)$ on subinterval i as given below equations (3.2). Note functions $\mathbf{h}^{(i)}(z)$ satisfy the same boundary conditions as $\mathbf{C}^{(i)}(z)$ (their definition would change for different boundary condition types) with $\dfrac{d^2}{dz^2}\mathbf{h}^{(i)}(z) = 0$. Thus, on each subinterval, we obtain

$$\kappa_j \frac{d^2}{dz^2} D_j^{(i)}(z) = -f_j(\mathbf{D}^{(i)}(z) + \mathbf{h}^{(i)}(z); \mathbf{V}(z)) = F_j(\mathbf{D}^{(i)}(z); \mathbf{V}(z)) \tag{3.5}$$

with boundary conditions $\mathbf{D}^{(i)}(z_{\ell_i}) = \mathbf{D}^{(i)}(z_{r_i}) = \mathbf{0}$.

To solve equations (3.5), we employ an integral equation formulation obtained from the Greens function solution [4], writing

$$\mathbf{D}^{(i)}(z) = \int_{z_{l_i}}^{z_{r_i}} G_i(z,s)\mathbf{F}(\mathbf{D}^{(i)}(s); \mathbf{V}(s))ds, \tag{3.6}$$

where the Green's function $G_i(z,s)$ for this system (with Dirichlet boundary condtions at 0 and L) is given by

$$G_i(z,s) = \begin{cases} \dfrac{1}{\kappa_i}\dfrac{(z - z_{l_i})(s - z_{r_i})}{z_{r_i} - z_{l_i}} & z_{l_i} \le z \le s \le z_{r_i} \\ \dfrac{1}{\kappa_i}\dfrac{(z - z_{r_i})(s - z_{l_i})}{z_{r_i} - z_{l_i}} & z_{l_i} \le s \le z \le z_{r_i}. \end{cases}$$

Equation (3.6) is solved by the following fixed point iteration

$$\mathbf{D}^{(i)}_{(k+1)}(z) = \int_{z_{l_i}}^{z_{r_i}} G_i(z,s)\mathbf{F}(\mathbf{D}^{(i)}_{(k)}(s);\mathbf{V}(s))ds, \tag{3.7}$$

where $\mathbf{D}^{(i)}_{(k)}(z)$ is the k-th iteration. The numerical approximation at grid point $z^{(i)}_\mu = z_{l_i} + \mu h, 1 \le \mu \le N$, where $h = \dfrac{L}{pN+1}$ is the mesh size, is obtained by approximating integral (3.7) by numerical quadrature

$$\begin{aligned} \mathbf{D}^{(i)}_{(k+1)}(z^{(i)}_\mu) &= \int_{z_{l_i}}^{z_{r_i}} G_i(z^{(i)}_\mu, s)\mathbf{F}(\mathbf{D}^{(i)}_{(k)}(s),\mathbf{V}(s))ds \\ &\approx h\left(\sum_{\nu=1}^{N} w_\nu G_i(z^{(i)}_\mu, z^{(i)}_\nu)\mathbf{F}(\mathbf{D}^{(i)}_{(k)}(z^{(i)}_\nu);\mathbf{V}(z^{(i)}_\nu))\right), \end{aligned} \tag{3.8}$$

where w_ν are the weights of a quadrature rule (we use the multiple Simpson's rule), and where for simplicity we present the case of one of the "interior" intervals. By defining the $N \times N$ matrix G with $G_{\mu\nu} = G_i(z^{(i)}_\mu, z^{(i)}_\nu)$ (note this value is independent of i as long as each subinterval has the same size with same number of evenly distributed grid points, as is the case here), the $N \times N$ diagonal matrix W with diagonal entry $W_{\nu\nu} = w_\nu h$, the $N \times 1$ vector $\mathbf{D}^{(i)}_{(k)}$ with $\mathbf{D}^{(i)}_{(k),\mu} = \mathbf{D}^{(i)}_{(k)}(z^{(i)}_\nu)$, and the $N \times 1$ vector $\mathbf{F}(\mathbf{D}^{(i)}_{(k)};\mathbf{V}^{(i)})$ with $\mathbf{F}(\mathbf{D}^{(i)}_{(k)};\mathbf{V}^{(i)}))_\nu = \mathbf{F}(\mathbf{D}^{(i)}_{(k)}(z^{(i)}_\nu);\mathbf{V}(z^{(i)}_\nu))$, then the iterative method given by (3.8) can be written in the matrix-vector form

$$\mathbf{D}^{(i)}_{(k+1)} = GW \cdot \mathbf{F}(\mathbf{D}^{(i)}_{(k)};\mathbf{V}^{(i)})) \tag{3.9}$$

Using definition (3.3), the iterative scheme for the original unkown $\mathbf{C}^{(i)}$ is then

$$\mathbf{C}^{(i)}_{(k+1)} = -GW \cdot \mathbf{f}(\mathbf{C}^{(i)}_{(k)};\mathbf{V}^{(i)})) + \mathbf{h}^{(i)}_{(k)}. \tag{3.10}$$

Pseudo code is provided in Algorithm 1, where the numerical solution at the $k-$th iteration on the entire domain $[0, L]$, $\mathbf{C}_{(k)}$, is a vector of length $pN + 2$ with concatenated subintercal approximations $\mathbf{C}^{(i)}_{(k)}, 1 \le i \le p$. Note that $\mathbf{C}_{(k)}$ satisfies the boundary conditions at $z = 0, L$. The L_2 norm is used for calculating the error between two consecutive iterations.

Algorithm 1: Pseudo code for domain decomposition method

Initialization: $tol = 10^{-5}, K_{MAX} = 10^3, i_{max} = 2, error = 1, k = 0$, also set initial guess for the unknowns $\mathbf{C}_{(0)}^{(i)}, 1 \leq i \leq p$

while $error > tol$ and $k < K_{MAX}$ **do**

  for $i = 1 : p$ **do**

    Define $\mathbf{h}_{(k)}^{(i)}$ by (3.4) using values of $\mathbf{C}_{(k)}^{(i)}$

    $\tilde{\mathbf{C}}_{old} = \mathbf{C}_{(k)}^{(i)}$

    for $iter = 1 : i_{max}$ **do**

      $\tilde{\mathbf{C}}_{new} = -GW \cdot \mathbf{f}(\tilde{\mathbf{C}}_{old}; \mathbf{V}^{(i)})) + \mathbf{h}_{(k)}^{(i)}$

      $\tilde{\mathbf{C}}_{old} = \tilde{\mathbf{C}}_{new}$

    end

    $\mathbf{C}_{(k+1)}^{(i)} = \tilde{\mathbf{C}}_{new}$

  end

  $error = ||\mathbf{C}_{(k+1)} - \mathbf{C}_{(k)}||_{L^2}$

  $k = k + 1$

end

It follows from either (3.9) or (3.10) that we are facing a fixed point problem. As is well known, convergence to a unique fixed point follows if the operator is a contraction; see, e.g., [8, 28]. We state the appropriate theorem for our particular situation:

THEOREM 3.1. *Let* $\mathbf{f}(\mathbf{Y}; \mathbf{V})$ *be such that there exists a matrix* $\mathbf{K}$ *with the property that* $|\mathbf{f}(\mathbf{Y_1}; \mathbf{V}) - \mathbf{f}(\mathbf{Y_2}; \mathbf{V})| \leq \mathbf{K}|\mathbf{Y_1} - \mathbf{Y_2}|$*, for all pairs* $\mathbf{Y_1}, \mathbf{Y_2}$*, where the absolute value is understood componentwise. If there is a norm for which* $\|GW\mathbf{K}\| < 1$*, then, the fixed point iteration* $\mathbf{Y}_{(k+1)} = -GW\mathbf{f}(\mathbf{Y}_{(k)}; \mathbf{V}) + \mathbf{h}$ *converges to the unique fixed point for any initial value* $\mathbf{Y}_{(0)}$*.*

We know the matrices G and W, while $\mathbf{K}$ is problem dependent. In the case of Simpson's rule, then $\|W\| = \frac{1}{3}h$ and $h = L/(Np+1)$. The eigenvalues of the matrix G are known, since it is the inverse of a Toeplitz matrix [33], with maximum eigenvalue

$$\frac{h}{2}\left(1 - \cos\left(\frac{\pi}{N+1}\right)\right)^{-1}.$$

We conclude that if h is sufficiently small so that

$$\frac{h^2}{6}\left(1 - \cos\left(\frac{\pi}{N+1}\right)\right)^{-1}\|\mathbf{K}\| < 1, \tag{3.11}$$

then Algorithm 1 converges.

To finish this Section we remark that in [45] two other numerical methods were implemented for the GNEP studied here, namely, standard finite difference and shooting methods [19]. The Green's function based domain decomposition method was found to outperform these other two methods, producing, for similar computation times, an error of about half that of the finite difference method and three orders of magnitude smaller than the shooting method. Improvement in efficiency, possibly because Green's functions propagate changes quickly through entire domains (or subdomains), becomes important for expensive problems of the sort considered below. As a bonus,

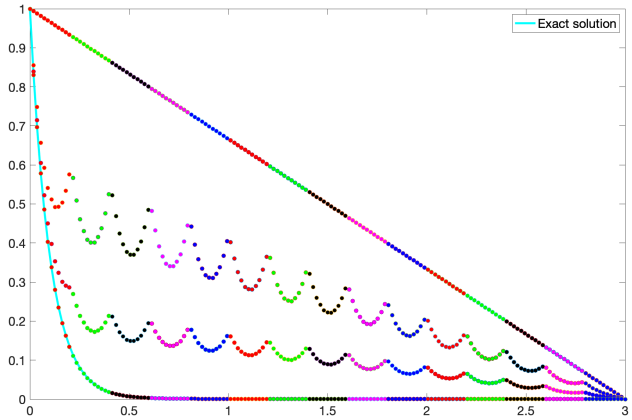

FIG. 4.1. *Approximated solution of equation (4.1) using domain decomposition. Here* $\kappa = -100$, $L = 3$, *and* $p = 15, N = 11$. *Initial guess is the linear function* $1 - z/3$. *From top to bottom: initial guess, first two iterates, final approximation to solution (4.2), all plotted as dotted curves, together with the exact solution which is plotted as a solid curve (indistinguishable by eye from the final approximation).*

domain decomposition lends itself to parallelization and further speed up, though we don't take advantage of this feature here.

4. A Simple Example. To illustrate the motivation for introducing domain decomposition, we start with a simple example, namely the "system"

$$\frac{d^2C}{dz^2} = -\kappa C,\ C(0) = 1,\ C(L) = 0, \tag{4.1}$$

with $z \in [0\ L]$, which can be interpreted as the case of a single species (or player type) with volume fraction $V = 1$, and a singleton strategy set $\mathcal{S}(z) = \{\kappa C(z)\}$. Though a singleton, $\mathcal{S}$ is still dependent on choices made by players at other locations.

We illustrate the proposed domain decomposition method, applying it to problem (4.1) using $\kappa = 100$ and $L = 3$, see Figure 4.1, with $p = 15, N = 11$, i.e., 15 subintervals and 11 interior grid points within each subinterval. For this problem, $\|\mathbf{K}\| = \kappa$, and the quantity in (3.11) is $\frac{3^2}{6\times 165^2}\frac{1}{0.0341}100 = 0.1617$, so that convergence is guaranteed. The initial guess, two intermediate solutions, and the final convergent solution were plotted (different colors distinguish different subdomains). For reference, the exact solution is given by

$$C(z) = \frac{\sinh(\sqrt{|\kappa|}(L - z))}{\sinh(\sqrt{|\kappa|}L)} = \frac{\sinh(30 - 10z)}{\sinh(30)}. \tag{4.2}$$

For large κ, problem (4.1) is stiff in z (large κ here means nondimensional length scale ratio $\sqrt{|\kappa|}L \gg 1$), and in fact the numerical scheme described above, without domain decomposition, does not converge, see Figure 4.2 (and note the scale of the vertical axis). In this case, condition (3.11) is not satisfied, and the hypotheses of Theorem 3.1 do not hold. The numerical solutions from the first two iterations show strong instability and departs far away from the exact solution (4.2). Thus we observe the need for domain decomposition even in this simple example.

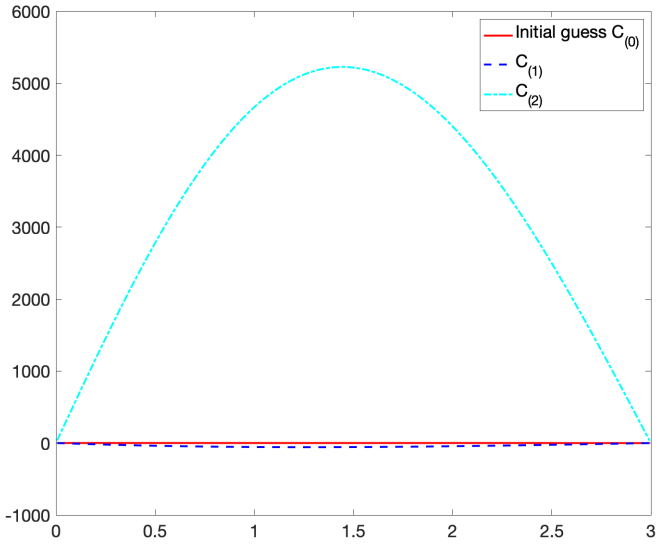

FIG. 4.2. *Attempted solution of equation (4.1) without domain decomposition. Here* $\kappa = -100$, $L = 3$, *and the domain is discretized with 500 grid points. Initial guess is the linear function* $1 - z/3$.

5. Biofilms. Our main focus is a biofilm model, consisting of transport equations of the form (2.1) for a collection of chemical concentrations $\mathbf{C}(z,t)$, coupled with growth-modulated transport equations for a collection of microbial species with volume fractions $\mathbf{V}(z,t)$ defined on an interval $[0\ L(t)]$, where $L(t)$ indicates biofilm depth [21, 26]. Vector $\mathbf{V}$ satisfies

$$\frac{\partial \mathbf{V}}{\partial t} + \frac{\partial}{\partial z}(u\mathbf{V}) = \mathbf{g}(\mathbf{C}, \mathbf{V}) \tag{5.1}$$

where component g_ℓ of $\mathbf{g}$ indicates the volumetric growth of species ℓ. We assume that $g_\ell = g_\ell(\mathbf{C})V_\ell$. Velocity $u = u(z,t)$, accounting for growth-induced expansion, is determined through the constraint $\sum_{\ell=1}^{m} V_\ell = 1$; in particular, summing the components of (5.1) results in equation

$$\frac{\partial u}{\partial z} = \sum_{\ell=1}^{m} g_\ell \tag{5.2}$$

for u. Supposing that the substratum at $z = 0$ is impenetrable, then equation (5.2) comes with boundary condition $u(0,t) = 0$, and so

$$u(z,t) = \int_0^z \sum_{\ell=1}^{m} g_\ell(s,t)\, ds.$$

The biofilm depth $L(t)$ obeys equation

$$\frac{dL}{dt} = u(L,t) - \sigma L^2 \tag{5.3}$$

where, in order to reach steady state, we include erosional term $-\sigma L^2$ of a form often used in biofilm models [1, 20]. Erosion is introduced here as a convenience to prevent unbounded biofilm growth.

In traditional phenomenonological models, the growth functions g_ℓ are functions (often linear) of the flux functions f_j, e.g., growth rate of organism ℓ at location $\mathbf{x}$ is proportional to flux rate, at $\mathbf{x}$, of oxygen into that organism. We allow a more general determination here, including calculating growth using intracellular reactions fluxes $\boldsymbol{\alpha}$, see (5.6), determined from player strategies.

Note that the biofilm model domain $z \in [0\ L(t)]$ involves a moving boundary at $L(t)$. For numerical purposes below, we transform to a coordinate $\zeta = z/L(t)$ in order to obtain a fixed computational domain $\zeta \in [0, 1]$, as is a common practice for 1D biofilm models. (Details of the transformation, as well as of the solution methodology used below, can be found in [46, 47].) The transformed versions of equations (3.1) and (5.1)-(5.3) are solved, as a system, for $\zeta \in [0, 1]$, and results are reported on the original spatial domain $z \in [0, L]$. See Section 5.2 for an example. An example with a very simplified ecology and metabolism (one species and three chemical concentrations) can be found in [47].

5.1. Metabolic Constraints. Volume fraction equations (5.1) are coupled to chemical transport equations

$$\kappa_j \frac{d^2}{dz^2} C_j(z) = -\sum_{\ell=1}^{m} F_{j,\ell}(\mathbf{C}) V_\ell \tag{5.4}$$

for concentrations C_j, $j = 1, 2, \ldots, n$. The source/sink terms on the righthand sides of these equations and, in particular, the strategy vectors

$$[\, F_{1\ell}(\mathbf{C}(z))\ F_{2\ell}(\mathbf{C}(z))\ \ldots\ F_{n\ell}(\mathbf{C}(z))]$$

at location z of species ℓ, are chosen from possible strategy sets defined by constraints on the individual fluxes $F_{j\ell}(z)$.

These constraints come in different forms. First, fluxes $F_{j,\ell}$ may be required to satisfy bounds

$$L_{j,\ell}(C_j) \le F_{j,\ell} \le U_{j,\ell}(C_j), \tag{5.5}$$

enforcing bounds on flux into or out of cells. For example, $L_{j,\ell} = -\mu_{j\ell} C_j$ (first order form) or $L_{j,\ell} = -\mu_{j\ell} C_j (K_{j\ell}+C_j)^{-1}$ (Monod form) are common choices. These bounds are a consequence of physical (e.g., transport limitation) or kinetic (e.g., transporter copy nunber) constraints.

A second type of commonly prescribed constraint enforces flux balance. That is, net fluxes of metabolic reaction products must balance [34]. Most metabolite fluxes arise from reactions internal to cells, and are thus not explicitly tracked in (5.4); however they are coupled to fluxes $F_{j,\ell}$, which for purposes of this discussion we call *exchange fluxes* as they measure exchanges of metabolites from inside to outside of cells. Supposing a metabolic steady state, that is, supposing that concentrations of internal metabolites are constant in time, then reaction fluxes creating and depleting any given internal metabolite concentration must balance. This results in a constraint which is linear in the vector of reaction fluxes, and takes the form

$$N_\ell^{(\mathrm{int})} \boldsymbol{\alpha}_\ell = N_\ell^{(\mathrm{exch})} \mathbf{F}_\ell\,, \tag{5.6}$$

where $\boldsymbol{\alpha}_\ell$ is the vector of internal reaction fluxes for species ℓ, $\mathbf{F}_\ell$ is the vector of exchange fluxes for species ℓ (with components $F_{j,\ell}$), and the rows of matrices $N_\ell^{(\text{int})}$ and $N_\ell^{(\text{exch})}$ containing (known) stoichiometric coefficients for internal and exchange metabolic reactions of species ℓ. Equation (5.6) implies that $N_\ell^{(\text{exch})}\mathbf{F}_\ell$ is constrained to sit in the range of $N_\ell^{(\text{int})}$. The strategy set, then, for species ℓ at location $\mathbf{x}$ consists of vectors $\mathbf{C}$ with $N_\ell^{(\text{exch})}\mathbf{F}(\mathbf{C})$ lying in the range of matrix $N_\ell^{(\text{int})}$ and satisfying bounds (5.5) as well as any other requirements that might be placed on metabolic reactions (e.g., additional constraints, such as nonnegativity, may be imposed on components of $\boldsymbol{\alpha}_\ell$). See [22] for more details.

5.2. A Genome-Scale Example. For a concrete model system, we consider a skin-related microbial biofilm community consisting of two bacterial species, *Staphylococcus aureus* USA300 (*S. aureus*) and *Staphylococcus epidermidis* 12228 (*S. epidermidis*), with 33 dissolved external chemical concentrations (see Supplemental Material for the complete list) based on a modified version of Hussain-Hastings-White (HHW) medium [17]. Optimizations needed for functions $F_{j,\ell}$, see (5.4), and g_ℓ, see (5.1), are evaluated using flux balance analysis via the COBRA Toolbox v2.0 for Matlab [5, 9, 36] together with high-quality genome-scale metabolic models for *S. aureus* and *S. epidemidis* [38]. Here $\ell = 1, 2$ indexes the two species types and $j = 1, 2, \ldots, 33$ indexes the 33 chemical concentration types. That is, $F_{j,\ell}$ denotes exchange flux (per volume fraction) for species ℓ of chemical j. One technical remark: COBRA output reports exchange fluxes in mass units, specifically in mmol/gDW·hr (where gDW = gram dry weight), whereas the biofilm model equations are written in terms of volume fractions. A conversion factor α is thus required (units of gDW/m^3), which is dependent on an estimate of $0.33 \cdot 10^6$ grams dry weight per m^3 of cells [27], and conservative estimate of cell volume fraction 0.1 for biofilm taking into account extracellular material. That is, we use $\alpha = (0.1)(0.33 \cdot 10^6) \approx 3 \cdot 10^4$ gDW/m^3.

COBRA computes an optimized set of exchange fluxes $F_{j,\ell}$ based on local chemical conditions. (Often, and we follow the practice here, the optimization is based on maximizing organism growth rate, though other criteria are possible.) Each call to COBRA requires a user-supplied metabolic model, which involves a stoichiometric matrix N of the type described in Section 5.1. Metabolic models are mathematical representations of genome-enabled chemical reactions that facilitate computation and prediction of phenotypes through the optimization of an objective function under constraints. Central to these models are lists of metabolites (chemicals) and gene-encoded enzyme-catalyzed reactions for which these metabolites are reactants and products. The *S. aureus* model we employ consists of 866 genes, 1121 metabolites, and 1377 reactions, of which 188 are designated as exchange reactions (that is, flux through the reaction actually consists of metabolites entering or exiting cells) while that of *S. epidermidis* consists of 755 genes, 1059 metabolites, and 1246 reactions, of which 167 are exchange reactions. Under simulations conditions, only a subset of exchange reactions are active, that is, exhibit non-zero flux above round-off levels; these constitute the 33 external concentrations that are tracked via equations of the form (5.4). Note that internal metabolite concentrations are unknown; however, FBA (and COBRA) requires that they be *flux-balanced*, that is, production and usage rates must balance for each internal metabolite. Satisfying this requirement, as well as other constraints (e.g., bounds on flux through a given reaction) results in a set of allowable metabolic strategies.

At each location within the biofilm domain and at each moment in time, each

organism is provided with an optimized metabolic strategy as provided by COBRA. This strategy is dependent on the local chemical concentration profile, together with constraints (as described below). However, the chemical concentration profile at any given point depends simultaneously on the metabolic strategies employed throughout the biofilm. Finding, at a given time, a consistent set of strategies and chemical profiles, i.e., a solution to the system (5.4), can then be interpreted as finding a generalized Nash equilibrium. Note that, for purposes here, COBRA can be considered as a "black box", or indeed replaced by some other black box, which, given local conditions such as chemical concentrations, chooses an optimal organism strategy for chemical consumption and production from whatever is designated the allowable set.

For the solution of equations (5.4), diffusion coefficients κ_j are chosen based on literature values for the most part, with a few estimated, see Supplemental Material. Monod-type bounds are applied exchange reaction fluxes from extracellular regions to intracellular regions, e.g., oxygen exchange flux is constrained by

$$v_{\mathrm{O}_2,\mathrm{exchange}}(z) \geq -r_{\max}\frac{C_{\mathrm{O}_2}(z)}{K_{\mathrm{O}_2}+C_{\mathrm{O}_2}(z)} \tag{5.7}$$

where $C_{\mathrm{O}_2}(z)$ is the extracellular oxygen concentration at location z. The negative sign indicates the convention that flux out of cells is designated as positive. Positive exchange flux is not constrained. Half-saturation concentrations are not generally available in the literature to our knowledge, so, for substrate α, we set K_α to be half of its non-zero Dirichlet boundary condition. Chemicals that only occur as byproducts are assigned homogeneous Dirichlet boundary conditions at each boundary, but are only produced by cells and hence lower bounds (5.7) are not relevant. Maximum flux coefficients $r_{\max}$ are estimated based on growth experiments performed for *S. aureus* [38]

Boundary conditions are chosen to mimic removal (homogeneous Dirichlet) or supply (non-homogeneous, positive Dirichlet) of chemicals through the biofilm boundary. Oxygen takes non-zero value 0.4 mmol at $z = L(t)$ (approximate value for lab conditions), the top of the biofilm domain, and zero value at $z = 0$, the bottom. Metabolic byproducts, including ethanol, take value of 0 at both boundaries where they are removed from the system. The remaining chemicals are metabolic substrates, introduced from the bottom of the biofilm and removed from the top (i.e., take non-zero Dirichlet confidition at $z = 0$ and zero Dirichlet condition at $z = L$). The non-zero boundary coefficient is chosen in proportion to abundance in HHW media, with glucose taking boundary concentration 55.5 mmol (following [17]), except for three chemicals that were found to be necessary to supplement HHW medium to allow growth (namely molybdate, putrescine, and zinc ion) which each were given boundary concentration 1 mmol. See Supplemental Material for further details.

The two organisms we follow, *S. aureus* and *S. epidermidis* are relevant to skin-related microbial communities, for which, roughly, oxygen is supplied (mostly) from above and other chemicals enter and exit (mostly) from below. Our set-up models a related lab technique called the colony biofilm method in which biofilm is grown with a nutrient-infused agar base below and with air exposure above [3]. In this geometry, once the biofilm has grown to be sufficiently thick, diffusive transport limitation can be expected to lead to an anaerobic zone at the bottom of the biofilm [2]. This is in fact what is observed in our computations. In Figure 5.1, we show profiles for 3 of the 33 external chemical concentrations for an 80 hour simulation. Horizontal axes are in time (hrs) and each vertical plot slice measures a property of a vertical slice

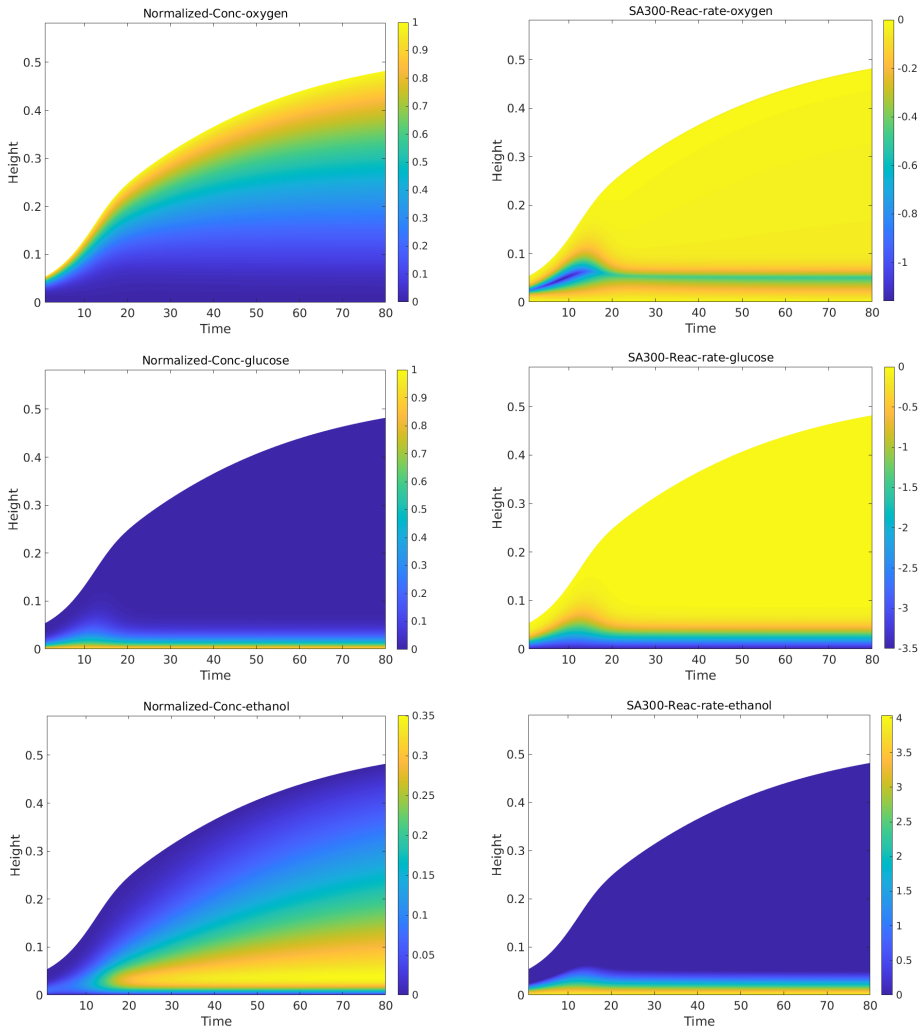

FIG. 5.1. *Biofilm simulation with limiting O_2 and glucose. In total, 33 external metabolites are tracked; concentrations and usage rates are shown for oxygen, glucose, and ethanol. Initial depth is 5 μm. Oxygen concentration (scaled units, with $1 = 0.4$ mmol) is set to be 1 at the top of the biofilm and 0 at the bottom at all times. Glucose concentration (scaled units, with $1 = 55.5$ mmol) is set to be 0 at the top of the biofilm and 1 at the bottom at all times. Ethanol concentration (scaled units, with $1 = 111$ mmol) is set to be 0 at both top and bottom of the biofilm at all times. Horizontal axes are time (hrs) and vertical axes are transverse height in the biofilm (10^2 μm). Top left: oxygen concentration (external to cells). Middle left: glucose concentration (external to cells). Bottom left: ethanol concentration (external to cells). Top right: oxygen usage rate. Middle right: glucose usage rate Bottom right: ethanol production rate Simulations suggests that there is a fermentation layer (glucose to ethanol) at the bottom of the biofilm, where oxygen concentration is low. Other parameters. Scaling: lengths are scaled by 100 μm, i.e., $z = 1$ indicates 100 μm, and times are scaled in units of hours, i.e., $t = 1$ indicates 1 hr. Initial conditions: initial biofilm thickness is 5 μm, initial volume fractions for the two bacterial species are both 0.5 across the entire spatial domain. Numerical parameters: the parameter σ in the erosional term $-\sigma L^2$ is set to 0.1. The domain decomposition parameters are $p = 30$ (number of subdomains), $N = 5$ (number of interior grid points in each subdomain). Time step size is $\Delta t = 0.05$. Note thus the total simulation time 80 results in 1600 total time steps.*

of the biofilm at that given time. Note the increasing height of the colored regions indicates biofilm growth. In this simulation, glucose is fed into the biofilm from the bottom and oxygen enters from the top. Three metabolic layers are evident. We see a layer of glucose fermentation at the bottom, with ethanol produced as a byproduct, where oxygen concentration is low. Above the fermentation layer, where oxygen is able to diffuse from the upper biofilm boundary, glucose is respired until the oxygen is depleted. Above the respiration layer, little activity occurs.

Note that there is also a change in metabolic pattern at approximately $t = 12$ hrs, where the biofilm transitions from thin to thick. At early times, oxygen is able to diffuse almost to the bottom of the biofilm (not quite all the way to the bottom, in quantity, because of the zero boundary condition at $z = 0$), so relatively little glucose is consumed by fermentation. At later times, when the biofilm becomes thick, diffusive transport limitation reduces oxygen flux near the bottom of the biofilm with the result that most glucose is fermented in a layer of fixed depth.

6. Discussion. Motivated by the metabolism and ecology of microbial communities, we have identified a system of continuously distributed (in space) agents, coupled through diffusing resources and byproducts, as a generalized Nash equilibrium problem. The underlying mathematical system that results consists of a system of nonlinearly coupled elliptic transport equations to which standard PDE methods can be applied. This connection is useful; for example, we can apply available methods to compute Nash equilibria. Here we have employed a domain decomposition approach. There are of course other possibilities, e.g., variational methods.

There are a number of further issues. Notably, we do not address uniqueness of solutions, a question of some interest in application. Bistable (or multistable) community metabolism could imply that not only current environment but also environmental history are important. Further, in the model system we study, agents act only with knowledge of their local environment. In actual microbial communities, chemical signals of various sorts may provide nonlocal information and even the possibility of cooperative, nonlocal strategies. Again, we have not considered these possibilities.

The system studied here turns out to be stiff in a certain sense; small changes in metabolic activity in one location in the domain can introduce numerical instability due to significant induced changes in other locations. The culprit is rapid decay (in space) of limiting chemical concentrations, specifically of oxygen in our model example, but similar rapid concentration changes are to be expected generally. In response, we have used a domain decomposition methodology which mitigates nonlocal coupling by, essentially, introducing multiscale interactions between agents. Note that domain decomposition has the further advantage of providing a foundation for parallelizing computations, though we do not explore that feature here.

Acknowledgements. The authors acknowledge support via NSF/DMS 1517100, 1951532 and 2325170.

7. Appendix: Existence of Solutions. We consider existence of solutions for equations (2.1) equiped with domain and boundary conditions such that each operator $\mathcal{L}_j$ has a Greens function solution [4]. That is, we suppose that each equation

$$\mathcal{L}_j C_j = g(\mathbf{x}),\ j = 1, \ldots, n,$$

together with its assigned boundary conditions, has a unique solution if g is smooth. It is a straightforward exercise, see for example [10], to then show that the nonlinear

system (2.1) then has a solution, though not necessarily unique, if the functions f_j are smooth and bounded. Metabolism is bounded, both in practice and in models, but modeled versions are not necessarily smooth as metabolic strategies can change discontinuously with change in local chemical concentrations. One can argue that, in the microbial community setting, this discontinuity should be smoothed by metabolic variations between individual microbes, e.g., averaging over variability between individuals in Monod coefficients as in (5.7) smooths metabolic strategy discontinuities.

We might wish to also consider, though, the possibility of existence of solutions to this system when the functions $f_j(\mathbf{C})$ are piecewise smooth in $\mathbf{C}$, defined here to mean that the functions $f_j(\mathbf{C})$ are smooth in the nonnegative orthant of $\mathbb{R}^n$ except on a piecewise smooth manifold Γ. We define smoothed approximations $f_j^{(\epsilon)}(\mathbf{C})$ such that $f_j^{(\epsilon)}(\mathbf{C})$ is itself smooth, satisfying the same bounds as $f_j(\mathbf{C})$, and such that $f_j^{(\epsilon)}(\mathbf{C}) = f_j(\mathbf{C})$ except for values $\mathbf{C}$ within distance ϵ of Γ. Note that equations

$$\mathcal{L}_j C_j^{(\epsilon)} = f_j^{(\epsilon)}(\mathbf{x}),\ j = 1, \ldots, n,$$

have a smooth solution $\mathbf{C}^{(\epsilon)}$ for each ϵ. As a consequence of the Arzela-Ascoli Theorem, there exists a convergent sequence $\mathbf{C}^{(\epsilon_k)} \to \mathbf{C}^{(0)}$ with $\epsilon_k \to 0$ as $k \to \infty$. For each solution $\mathbf{C}^{(\epsilon_k)}$, we have

$$C_j^{(\epsilon_k)}(z) = \int_0^L G_j(z;\hat{z}) f_j^{(\epsilon_k)}(\mathbf{C}^{(\epsilon_k)}(\hat{z}))d\hat{z},\ j = 1, \ldots, n, \tag{7.1}$$

where $G_j(z;\hat{z})$ is the Greens function for operator $\mathcal{L}_j$ (including its boundary conditions). Note that $f_j^{(\epsilon_k)}(\mathbf{C}^{(\epsilon_k)}(z)) \to f_j(\mathbf{C}^{(0)}(z))$ for values of z such that $\mathbf{C}^{(0)}(z)$ does not lie in Γ, and hence, if intersections with Γ are isolated, we can take the limit $k \to \infty$ in (7.1) to obtain

$$C_j^{(0)}(z) = \int_0^L G_j(z;\hat{z}) f_j(\mathbf{C}^{(0)}(\hat{z}))d\hat{z},\ j = 1, \ldots, n.$$

That is, $\mathbf{C}^{(0)}$ is a solution of system (2.1).

REFERENCES

[1] F. Abbas, R. Sudarsan, R., H.J. Eberl, Longtime behavior of one dimensional biofilm models with shear dependent detachment rates, *Math Biosci Eng* **9**, (2012), pp. 215–289.

[2] S, Abdul Rani, B. Pitts, H. Beyenal, R.A. Veluchamy, Z. Lewandowski, W,M. Davison, K. Buckingham-Meyer, P.S. Stewart, Spatial patterns of DNA replication, protein synthesis, and oxygen concentration within bacterial biofilms reveal diverse physiological states, *J. Bacteriol.* **189**, 4223-4233 (2007).

[3] J,N. Anderl, M.J. Franklin, P.S. Stewart, Role of antibiotic penetration limitation in *Klebsiella pneumoniae* biofilm resistance to ampicillin and ciprofloxacin, *Antimicrob. Agents Chemother.* **44**m 1818-1824 (2000).

[4] G. Barton, *Elements of Green's functions and propagation: potentials, diffusion, and waves*, Oxford University Press, Oxford, 1989.

[5] S.A. Becker, A.M. Feist, M.L. Mo, G. Hannum, B.Ø. Palsson, M.J. Herrgard, Quantitative prediction of cellular metabolism with constraint-based models: the COBRA Toolbox, *Nat Protoc* **2**, (2007), pp. 727–738.

[6] A. Bensoussan, R. Glowinski, J.-L. Lions, Méthode de décomposition appliquée au contrôle optimal de systèmes distribués, in *Proceedings of the 5th Conference on Optimization Techniques, Part 1*, Lecture Notes in Computer Science **5**, R. Conti, A. Ruberti, Eds., Springer, Berlin, (1973), pp. 141–151.

[7] J. Chen, J.A. Gomez, K. Höffner, P. Phalak, P.I. Barton, M.A. Henson, Spatiotemporal modeling of microbial metabolism, *BMC Syst Biol* **10**, (2016), pp. 1–13.
[8] L.B. Ciric, Generalized contractions and fixed-point theorems, *Publications de l'Institut Mathématique (Beograd)(NS)*, **12**, (1971), pp. 19–26.
[9] A. Ebrahim, J.A. Lerman, B.Ø. Palsson, D.R. Hyduke, COBRApy: COnstraints-Based Reconstruction and Analysis for Python, *BMC Syst Biol* **7**, (2013), Article number 74.
[10] L.C. Evans, *Partial Differential Equations*, Graduate Studies in Mathematics, Vol. 19, American Mathematical Society, Providence, Rhode Island 1998.
[11] F. Facchinci, C. Kanzow, Generalized Nash equilibrium problems, *Ann Oper Res* **175**, (2010), pp. 177–211.
[12] E. Frey, Evolutionary game theory: Theoretical concepts and applications to microbial communities, *Physica A* **389**, (2010), pp. 4265–4298.
[13] A. Frommer, D.B. Szyld, On asynchronous iterations, *J Comput Appl Math* **123**, (2000), pp. 201–216.
[14] C. Glusa, E. G. Boman, E. Chow, S. Rajamanickam, D. B. Szyld, Scalable Asynchronous Domain Decomposition Solvers, *SIAM J Sci Comput* **42**, (2007), pp. C384–C409.
[15] W.R. Harcombe, W.J. Riehl, I. Dukovski, B.R. Granger, A. Betts, A.H. Lang, G. Bonilla, A. Kar, N. Leiby, P. Mehta, C.J. Marx, D. Segrè, Metabolic resource allocation in individual microbes determines ecosystem interactions and spatial dynamics, *Cell Rep* **7**, (2014), pp. 1104–1115.
[16] F.J.H. Hol, P. Galajda, K. Nagy, R.G. Woolthuis, C. Dekker, J.E. Keymer, Spatial structure facilitates cooperation in a social dilemma: empirical evidence from a bacterial community, *PLOS One* **8**, (2013), e77042.
[17] M. Hussain, J.G.M. Hastings, P.J. White, A chemically defined medium for slime production by coagulase-negative staphylococci, *J. Med. Microbiol.* **34**, (1991), pp. 143-147.
[18] N. Jayasinghe, A. Franks, K.P. Nevin, R. Mahadevan, Metabolic modeling of spatial heterogeneity of biofilms in microbial fuel cells reveals substrate limitations in electrical current generation, *Biotech. J.* **9**, (2014), pp. 1350–1361.
[19] H.B. Keller, *Numerical Methods for Two-Point Boundary-Value Problems*, Blaisdell Publishing Co., Waltham, Mass. (1968).
[20] I. Klapper, Productivity and equilibrium in simple biofilm models, *Bull. Math. Biol.* **74**, (2012), pp. 2917–2934.
[21] I. Klapper, J. Dockery. Mathematical Description of Microbial Biofilms, *SIAM Rev* **52**, (2010), pp. 221–265.
[22] I. Klapper, D.B. Szyld, K. Zhao, *Metabolic Networks, Elementary Flux Modes, and Polyhedral Cones*, SIAM, Philadelphia 2021.
[23] J.U. Kreft, Biofilms promote altruism. *Microbiology* **150**, (2004), pp. 2751-2760.
[24] F. Magoulès, D.B. Szyld, C. Venet, Asynchronous optimized Schwarz methods with and without overlap, *Numer Math* **137**, (2017), pp. 199–227.
[25] R. Mahadevan, J.S. Edwards, F.J. Doyle III, Dynamic flux balance analysis of diauxic growth in *Escherichia coli*, *Biophys J* **83**, (2002), pp. 1331–1340.
[26] M.R. Mattei, L. Frunzo, B. D'Acunto, Y. Pechaud, F. Pirozzi, G. Esposito, Continuum and discrete approach in modeling biofilm development and structure: a review, *J Math Biol* **76**, (2018), pp. 945–1003.
[27] R. Milo, R. Phillips, N. Orme, Cell Biology By The Numbers, http://book.bionumbers.org (2015).
[28] J.M. Ortega, W.C. Rheinboldt, Iterative Solution of Nonlinear Equations in Several Variables, Academic Press, New York and London 1970. Reprinted by SIAM, Philadelphia 2000.
[29] J.D. Orth, I. Thiele, B.Ø. Palsson, What is flux balance analysis?, *Nat Biotechnol* **28**, 245–248 (2010).
[30] P. Phalak, J. Chen, R.P. Carlson, M.A. Henson, Spatiotemporal metabolic modeling of a chronic wound biofilm consortium, IFAC-PapersOnLine 49-26, (2016), pp. 032–037.
[31] E.E. Prudencio, R. Byrd, X.-C. Cai, Domain Decomposition Methods for PDE Constrained Optimization Problems, in *High Performance Computing for Computational Science - VECPAR 2004*, M. Daydé, J. Dongarra, V. Hernández, J.M.L.M. Palma, Eds., Lecture Notes in Computer Science, Vol. 3402, Springer, Berlin, (2005), pp. 569–582.
[32] E.E. Prudencio, X.-C. Cai, Parallel multilevel restricted Schwarz preconditioners with pollution removing for PDE-constrained optimization, *SIAM J Sci Comput* **29**, (2007), pp. 964–985.
[33] L. Reichel, L. N. Trefethen, Eigenvalues and pseudo-eigenvalues of Toeplitz matrices, *Linear Algebra Appl* **162**, (1992), pp. 153–185.
[34] J.A. Roels, Application of macroscopic principles to microbial metabolism, *Biotechnol. Bioeng.* **22**, (1980), pp. 2457-2514.

[35] E, Ruppin, J.A. Papin, L.F. de Figueiredo, S. Schuster, Metabolic reconstruction, constraint-based analysis and game theory to probe genome-scale metabolic networks, *Curr Opin Biotechnol* **21**, (2010), pp. 502–510.

[36] J. Schellenberger, R. Que, R.M.T. Fleming, I. Thiele, J.D. Orth, A.M. Feist, D.C. Zielinski, A. Bordbar, N.E. Lewis, S. Rahmanian, J. Kang, D.R. Hyduke, B.Ø. Palsson, Quantitative prediction of cellular metabolism with constraint-based models: the COBRA Toolbox v2.0, *Nat Protoc* **6**, (2011), pp. 1290–1307.

[37] S. Schuster, C. Hilgetag, On elementary flux modes in biochemical reaction systems at steady state, *J Biol Sys* **2**, (1994), pp. 165–182.

[38] Y. Seif, J.M. Monk, N. Mih, H. Tsunemoto, S. Poudel, C. Zuniga, J. Broddrick, K. Zengler, B.Ø. Palsson, A computational knowledge-base elucidates the response of *Staphylococcus aureus* to different media types, *PLOS Comp Biol* **15**, (2019), e1006644.

[39] B. Smith, P. Bjørstad, G. Gropp, *Domain Decomposition: Parallel Multilevel Methods For Elliptic Partial Differential Equations*, Cambridge University Press, Cambridge 2004.

[40] P.S. Stewart, M.J. Franklin, Physiological heterogeneity in biofilms, *Nat Rev Microbiol* **6**, (2008), 199210.

[41] G.D. Tartakovsky, A.M. Tartakovsky, T.D. Scheibe, Y. Fang, R. Mahadevan, D.R. Lovley, Pore-scale simulation of microbial growth using a genome-scale metabolic model: Implications for Darcy-scale reactive transport, *Adv Water Resour* **59**, (2013), pp. 256–270.

[42] A. Toselli, O. Widlund, *Domain Decomposition Methods-Algorithms And Theory*, Springer, New York 2006.

[43] M. Vulić, R. Kolter, Evolutionary cheating in *Escherichia coli* stationary phase cultures, *Genetics* **158**, (2001), pp. 519–526.

[44] Y. Xu, X. Chen, Optimized Schwarz methods for the optimal control of systems governed by elliptic partial differential equations, *J Sci Comp* **79**, (2019), pp. 1182–1213.

[45] X. Yu, A domain decomposition method for solution of a pde-constrained generalized nash equilibrium model of biofilm community metabolism. *PhD Dissertation* (2022).

[46] T. Zhang, B. Pabst, I. Klapper, P. S. Stewart, General theory for integrated analysis of growth, gene, and protein expression in biofilms, *PloS one* **8**, e83626 (2013).

[47] T. Zhang, A. Parker, R.P. Carlson, P.S. Stewart, I. Klapper, Multiscale flux-based modeling of biofilm communities, *Multiscale Model Simul* **18**, (2020), pp. 1025–1052.